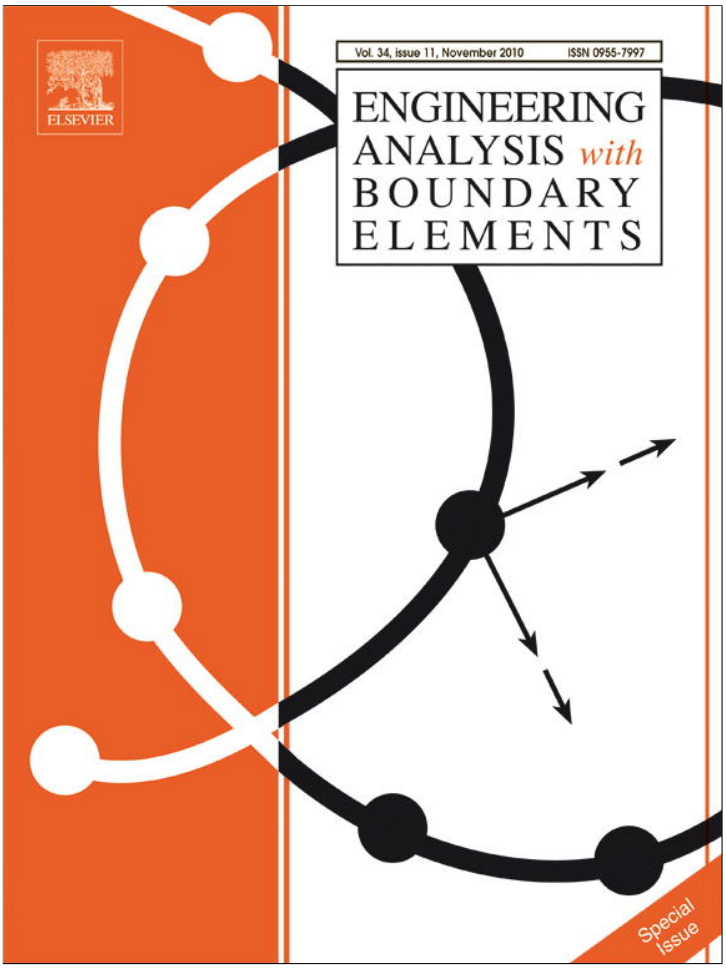

Engineering Analysis with Boundary Elements 34 (2010) 934–943

Contents lists available at ScienceDirect

Engineering Analysis with Boundary Elements

journal homepage: www.elsevier.com/locate/enganabound

An element implementation of the boundary face method for 3D potential problems

Xianyun Qin [a], Jianming Zhang [a,*], Guangyao Li [a], Xiaomin Sheng [a], Qiao Song [b], Donghui Mu [b]

[a] State Key Laboratory of Advanced Design and Manufacturing for Vehicle Body, College of Mechanical and Vehicle Engineering, Hunan University, Changsha 410082, China
[b] Beijing No.2 Machine Tool Works Co., Ltd., Beijing, China

ARTICLE INFO

Article history:
Received 29 March 2010
Accepted 11 April 2010
Available online 1 July 2010

Keywords:
BEM
Geometric map
Surface element
Boundary face method
CAD software

ABSTRACT

This work presents a new implementation of the boundary face method (BFM) with shape functions from surface elements on the geometry directly like the boundary element method (BEM). The conventional BEM uses the standard elements for boundary integration and approximation of the geometry, and thus introduces errors in geometry. In this paper, the BFM is implemented directly based on the boundary representation data structure (B-rep) that is used in most CAD packages for geometry modeling. Each bounding surface of geometry model is represented as parametric form by the geometric map between the parametric space and the physical space. Both boundary integration and variable approximation are performed in the parametric space. The integrand quantities are calculated directly from the faces rather than from elements, and thus no geometric error will be introduced. The approximation scheme in the parametric space based on the surface element is discussed. In order to deal with thin and slender structures, an adaptive integration scheme has been developed. An adaptive method for generating surface elements has also been developed. We have developed an interface between BFM and UG-NX(R). Numerical examples involving complicated geometries have demonstrated that the integration of BFM and UG-NX(R) is successful. Some examples have also revealed that the BFM possesses higher accuracy and is less sensitive to the coarseness of the mesh than the BEM.

1. Introduction

The boundary face method (BFM) has been implemented with shape functions from moving least-square (MLS) approximation [1]. Although the method has some attractive features in common with meshless methods [2–5] such as the hybrid boundary node method (HBNM) [3], it often encounters troubles when dealing with bodies with small holes and fillets. To solve problems involving domains with arbitrarily trimmed surfaces and to get better efficiency, this paper presents a new implementation with shape functions from boundary finite elements.

In the conventional BEM implementation of structural analyses, a geometric model is firstly built with a CAD package, the geometric model is then converted into a discrete model using a meshing tool. The CAD and BEM are treated as separate modulus requiring different methods and representations [6], which include continuous parametric models and discrete models, respectively. The elements are used for boundary integration and approximation of geometry in the BEM. Once the BEM model is constructed from CAD, the information of geometry is only derived from standard elements. Therefore, geometric errors are introduced. Moreover, the link between BEM model and CAD system is often unavailable, thus makes it difficult to carry out adaptive mesh refinement [7].

To cope with the problems above, we have developed the BFM [1]. A primary goal of our research is to make the computational model geometrically exact no matter how coarse the discretization is. Another goal is to simplify mesh refinement by eliminating the need for communication with the CAD geometry once the initial mesh is constructed. Yet another goal is to more tightly integrate the mesh generation process within CAD [7]. In our implementation, both boundary integration and variable approximation are performed on boundary faces, which are represented in parametric form exactly as the boundary representation data structure in most CAD systems. The parametric surface, which encapsulates the exact geometry of corresponding face, is discretized by surface elements in parametric space. These elements are used for the boundary integration and variable approximation. For boundary integration, however, the geometric data at Gaussian quadrature points, such as the coordinates, the Jacobian and the outward normal are calculated directly from the faces rather than elements, thus no geometric error will be introduced. The direct boundary integration and approximation in parametric space of surfaces forms an intrinsic feature of the BFM when compared with the conventional BEM.

* Corresponding author. Tel.: +86 731 88823061.
E-mail address: zhangjianm@gmail.com (J. Zhang).

0955-7997/$ - see front matter © 2010 Elsevier Ltd. All rights reserved.
doi:10.1016/j.enganabound.2010.04.009

The BFM is implemented directly on a solid modeling data structure, namely the boundary representation (B-rep). As the B-rep is used in most of CAD packages, it should be possible to exploit their Open Architecture feature, and automatically obtain required coefficients (representation). Therefore, our implementation has a real potential to seamlessly interact with CAD software, integrating easily geometric design and engineering analysis into a completely unified framework [6–8]. To show the advantageous features, we have developed an interface between BFM and UG-NX(R). Numerical examples have demonstrated that the integration of BFM and UG-NX(R) is successful, which may be an important step toward automatic simulation.

To deal with thin and slender structures effectively, an adaptive integration scheme for nearly singular integrals is developed. We have also developed an adaptive mesh generation method over an arbitrarily parametric surface based on the advancing front method (AFM) [9,10] combined with a quad-tree procedure. We have compared the presented method with the BEM with regard to accuracy, convergence and sensitivity of the results to the mesh density. Some examples that involving complicated geometry or small features are presented to verify the accuracy, efficiency and feasibility of the BFM. All results have shown very attractive features of the method.

The paper is organized as follows. In Section 2, the approximation scheme based on the surface element is described. Section 3 briefly describes the well-known BIE for potential problems. The adaptive face integration scheme is demonstrated in Section 4. Section 5 presented the adaptive mesh generation method. Numerical examples for 3-D potential problems are given in Section 6. The paper ends with conclusions in Section 7.

2. The approximation scheme in parametric space

As the BEM, the boundary of the 3-D solid is only needed for solving potential problems with the BFM. For the method, the boundary consists of a set of surfaces with parametric representation and the field variable approximation is performed in parametric space of each surface. This is a distinguishing feature between BFM and BEM.

As we known, a surface in physical space, Ω, is represented in parametric form as

$$\mathbf{r}(x,y,z)=\mathbf{r}(x(u,v),y(u,v),z(u,v))=\mathbf{r}(u,v) \tag{1}$$

where $\mathbf{r}$ is the position vector, and u and v are the parametric coordinates, which are constrained to the interval [0,1] mostly. The domain in parametric space corresponding to Ω is denoted by $\tilde{\Omega}$, and it is assumed that the map $F:\tilde{\Omega}\rightarrow\Omega$ by Eq. (1) is referred as a geometric map here. Since the geometric map is created, the shape function and its derivatives can be constructed over the parametric space $\tilde{\Omega}$. Then the subsequent variables in physical space at the parametric location (u, v) can be calculated using F, such as the coordinates (x, y, z).

In the parametric space $\tilde{\Omega}$, the methods using MLS [1] and NURBS [11] are proposed to approximate variable in success. With those methods, numerical results with better accuracy may be obtained, but the generality is lost when it needs to be extended to any trimmed surface [1,11]. In this paper, a simple but effective approximate method through Lagrange Polynomial is presented here, which is based on a surface element, similar to the standard Lagrange element [12]. The surface element is defined in the parametric space $\tilde{\Omega}$ of the surface. This is different from the element used in the conventional BEM.

To illustrate the approximation scheme, the quadrilateral surface element with four interpolating nodes in the space $\tilde{\Omega}$ (see Fig. 1) used for variable approximation is discussed in this paper. The element constructed by isocurves (the parametric line segment with constant coordinate value of u or v) is shown in Fig. 1(a), and Fig. 1(b) depicts the element consists of no isocurves.

The four interpolation functions associated with each node for the two types of elements above are given as follows:

$$\begin{aligned} &N_1=\frac{1}{4}(1+\xi)(1+\eta),\ N_2=\frac{1}{4}(1-\xi)(1+\eta)\\ &N_3=\frac{1}{4}(1-\xi)(1-\eta),\quad N_4=\frac{1}{4}(1+\xi)(1-\eta) \end{aligned}\qquad \xi,\ \eta\in[-1,1] \tag{2}$$

The shape functions are used to interpolate variables in both types of elements. With the method discussed in Ref. [12] on how to obtain derivatives of the shape function for isoparametric element, the derivatives $N_{k,u}$ and $N_{k,v}$ in the space $\tilde{\Omega}$ can be deducted easily. We omit the details for the sake of brevity. However, how to obtain parametric coordinates (u, v) responding (ξ,η) is different for both types of elements. For the first type of element (Fig. 1(a)), the parametric coordinates are obtained by the following simple linear transformation:

$$\begin{aligned} u&=0.5(u_b-u_a)+0.5(u_b+u_a)\xi\\ v&=0.5(v_b-v_a)+0.5(v_b+v_a)\eta \end{aligned} \tag{3}$$

While considering the second type of element (Fig. 1(b)), the parametric coordinates are also interpolated by the shape functions above as the follows:

$$u=\sum_{i=1}^{4}N_iu_i,\quad v=\sum_{i=1}^{4}N_iv_i \tag{4}$$

If we obtain the parametric coordinates (u, v) in the space $\tilde{\Omega}$ located at the surface element, the physical coordinates (x, y, z) in the space Ω can be calculated by the geometric map F. Consequently, a calculated point defined by these physical coordinates is located on the initial surface, and no geometric errors are introduced. It should be noted that the surface element constructed by parametric straight lines is usually made up of smooth curved edges in physical space Ω. So the need to employ isoparametric element defined in the space Ω to represent curved surface element is circumvented, thus avoiding complex mathematic transform needed for isoparametric element [12].

For the problems in potential theory, the independent boundary variables on the boundary of the solid to be solved are the potential and its normal gradient. Considering the geometric map F, these variables are interpolated by shape functions as

$$\begin{aligned} u(x,y,z)&=u(u,v)=u(\xi,\eta)=\sum_{k=1}^{N}N_k(\xi,\eta)u_k\\ q(x,y,z)&=q(u,v)=q(\xi,\eta)=\sum_{k=1}^{N}N_k(\xi,\eta)q_k \end{aligned} \tag{5}$$

where u_k and q_k are the nodal values of the potential and the normal gradient, N is the total number of interpolating nodes. The values of u and q for any field point in the surface element are only dependent on its nodal values and shape functions.

As we known, the CAD model is represented by NURBS usually and is not watertight in most cases due to the fact that gaps may appear in the interface of two NURBS surfaces [13]. This makes it unsuitable to place interpolating nodes at the edge of a surface where gaps occur. To deal with the problem, the strategy suggested by Kane [12] that allows both continuous and discontinuous elements to coexist in the same BEM model is

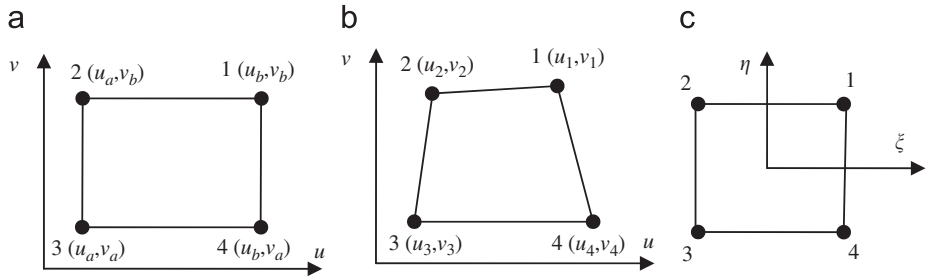

Fig. 1. Four-node surface elements: (a) rectangular element in parametric space; (b) quadrilateral element in parametric space and (c) coordinate mapping.

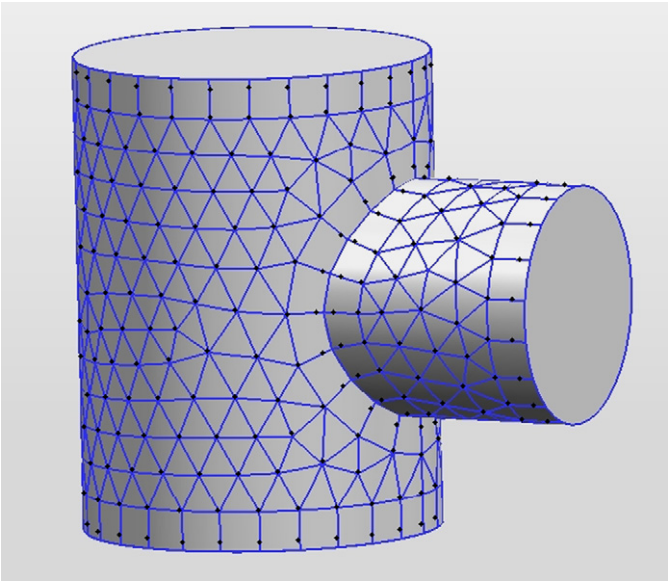

Fig. 2. Both continuous and discontinuous elements coexist in the same BFM model (elements on two adjacent surfaces are shown). Interpolating nodes are denoted by "●".

extended to be used in BFM. Discontinuous elements are employed along the boundary of a surface and continuous elements are adopted in the surface interior, thus there is not any interpolating node located at the surface edge as shown in Fig. 2. The procedure to obtain shape functions for any type of discontinuous element can be found in Ref. [12].

3. Boundary integral equations and integration issues

The potential problem in three dimensions governed by Laplace's equation with boundary conditions is written as

$$\begin{aligned} &u_{,ii}=0, && \forall x\in\Theta \\ &u=\overline{u}, && \forall x\in\Gamma_u \\ &u_{,i}n_i\equiv q=\overline{q}, && \forall x\in\Gamma_q \end{aligned} \tag{6}$$

where the domain Θ is enclosed by $\Gamma=\Gamma_u+\Gamma_q$, $\overline{u}$ and $\overline{q}$ are the prescribed potential and the normal flux, respectively, on the essential boundary Γ_u and on the flux boundary Γ_q, and n_i, $i=1,2,3$ are the components of the outward normal $\mathbf{n}$ direction to the boundary Γ.

The problem can be recast into an integral equation on the boundary. The well-known self-regular BIE for potential problems in 3-D is

$$0=\int_\Gamma (u(\mathbf{s})-u(\mathbf{y}))q^s(\mathbf{s},\mathbf{y})\,d\Gamma-\int_\Gamma q(\mathbf{s})u^s(\mathbf{s},\mathbf{y})\,d\Gamma \tag{7}$$

where $q=\partial u/\partial\mathbf{n}$, $\mathbf{y}$ is the source point and $\mathbf{s}$ is the field point on the boundary. $u^s(\mathbf{s},\mathbf{y})$ and $q^s(\mathbf{s},\mathbf{y})$ are the fundamental solution and its derivative, respectively. For 3-D potential problems,

$$u^s(\mathbf{s},\mathbf{y})=\frac{1}{4\pi}\frac{1}{r(\mathbf{s},\mathbf{y})} \tag{8}$$

$$q^s(\mathbf{s},\mathbf{y})=\frac{\partial u^s(\mathbf{s},\mathbf{y})}{\partial\mathbf{n}} \tag{9}$$

with r being the Euclidean distance between the source and field points.

The approximation scheme in the parametric space $\tilde{\Omega}$ derived in Section 2 will be used to approximate u and q on the boundary Γ. The bounding surface is discretized into elements in the space $\tilde{\Omega}$ face by face. These elements are generated by the advancing front method (AFM) [9,10] to be discussed in Section 5. Dividing Γ into N_E elements and substituting Eqs. (5) into (7), we have

$$\begin{aligned} 0=&-\sum_{j=1}^{N_E}\int_{\Gamma_j} q^s(\mathbf{s},\mathbf{y})\sum_{k=1}^{N}(N_k(\mathbf{s})-N_k(\mathbf{y}))u_k\,d\Gamma \\ &+\sum_{j=1}^{N_E}\int_{\Gamma_j} u^s(\mathbf{s},\mathbf{y})\sum_{k=1}^{N}N_k(\mathbf{s})q_k\,d\Gamma \end{aligned} \tag{11}$$

where $N_k(\mathbf{y})$ and $N_k(\mathbf{s})$ are the contributions from the kth interpolation node to the collocation point $\mathbf{y}$ and field point $\mathbf{s}$, respectively.

Eq. (11) can be put in a matrix form as

$$\mathbf{Hu}-\mathbf{Gq}=\mathbf{0} \tag{12}$$

where $\mathbf{u}$ and $\mathbf{q}$ contain the approximations to the nodal values of u and q at the boundary nodes. A well-posed boundary value problem can be solved using Eq. (12).

The first term on the right hand side of Eq. (11) is regular in any case. Therefore, regular Gaussian integration can be used to evaluate it over each element. However, special integration techniques are required for the second term, since it will become weakly singular as $\mathbf{s}$ approaches $\mathbf{y}$. When $\mathbf{y}$ and $\mathbf{s}$ belong to the same element, the element is treated as a singular element and the special techniques developed in the next section are used to carry out the integration. Our integration scheme is different from that developed by Chati and Mukherjee [14] and may provide better accuracy. This is because we carry out the integrations directly in the parametric space of a face rather than over elements, and thus no geometric error will be introduced.

Even when $\mathbf{y}$ and $\mathbf{s}$ belong to different element, they can still be very close to each other. In this case, the second term on the right hand side of Eq. (11) becomes nearly singular. This case occurs when thin structures are involved and when the distribution of elements is very irregular. We have also developed an adaptive scheme to calculate nearly singular integrals in the next section.

Since each surface element employed in our method is defined in the parametric space $\tilde{\Omega}$, the geometric map $F:\tilde{\Omega}\rightarrow\Omega$ is simultaneously preserved to calculate the integrand quantities in the physical space Ω in the process of the integration. The physical coordinates of integration point corresponding to the parametric values (u, v) are calculated by Eq. (1). According to the theory about parametric surface, the unit outward normal $\mathbf{n}(u, v)$ can be obtained by the following expression:

$$\mathbf{n}(u,v)=\frac{\mathbf{r}_u(u,v)\times\mathbf{r}_v(u,v)}{|\mathbf{r}_u(u,v)\times\mathbf{r}_v(u,v)|} \tag{13}$$

where $\mathbf{r}_u(u,v)$ and $\mathbf{r}_v(u,v)$ are tangent vectors at the point (u, v) over the surface, and the two vectors are defined as

$$\mathbf{r}_u(u,v)=\frac{\partial\mathbf{r}(u,v)}{\partial u}=\left(\frac{\partial x(u,v)}{\partial u},\frac{\partial y(u,v)}{\partial u},\frac{\partial z(u,v)}{\partial u}\right) \tag{14}$$

$$\mathbf{r}_v(u,v)=\frac{\partial\mathbf{r}(u,v)}{\partial v}=\left(\frac{\partial x(u,v)}{\partial v},\frac{\partial y(u,v)}{\partial v},\frac{\partial z(u,v)}{\partial v}\right) \tag{15}$$

in which other symbols have been defined in Eq. (1). And the Jacobian J_S of the geometric map F is given as

$$J_S=|\mathbf{r}_u(u,v)\times\mathbf{r}_v(u,v)| \tag{16}$$

Note that the integrand quantities for each integration point are derived from corresponding parametric surface by the geometric map F, making the computational geometry data to be exact. This is another distinguishing feature of BFM, when compared with conventional BEM in which the geometry data are approximated from elements.

4. Weakly and nearly singular integration schemes

4.1. Weakly singular integration

The second term on the right hand side of Eq. (11) becomes a weakly singular integral when **y** and **s** belong to a same element, and the element is treated as a singular element. There have been various methods proposed in the past to handle weakly singular integrals arising in BEM. Chati and Mukherjee have used a method suggested by Nagaranjan and Mukherjee [15] to carry out the weakly singular integration in BEM. Here we extended the method discussed in Ref. [1] to calculate singular integral occurred in arbitrary surface element in parametric space $\tilde{\Omega}$. The details are presented as follows.

To describe the problem, we take a quadrilateral surface element as an example here. If the element is not rectangular in shape in the space $\tilde{\Omega}$, as show in Fig. 3(a), a special coordinate transformation is applied to map it into an intrinsic coordinate system defined by (t_1, t_2) (see Fig. 3). Specially, if a surface element is constructed by isoparametric lines with rectangular shape in the parametric space, there is no need for this transformation.

Consider the weakly singular integral over the element as shown in Fig. 3(a). This can be represented as

$$I=\int_{patch}O(1/r)d\Gamma \tag{17}$$

Now, a square element in the intrinsic coordinate system can be divided into two, three or four triangles, depending on the location of the source point (on corner, edge or inside) (Fig. 3). To use Gaussian quadrature, the following mapping is used for each triangle (Fig. 4):

$$\begin{aligned}t_1^a&=t_1^0+(t_1^1-t_1^0)\alpha\\ t_2^a&=t_2^0+(t_2^1-t_2^0)\alpha\end{aligned} \tag{18a}$$

$$\begin{aligned}t_1^b&=t_1^0+(t_1^2-t_1^0)\alpha\\ t_2^b&=t_2^0+(t_2^2-t_2^0)\alpha\end{aligned} \tag{18b}$$

$$\begin{aligned}t_1&=t_1^a+(t_1^b-t_1^a)\beta\\ t_2&=t_2^a+(t_2^b-t_2^a)\beta,\end{aligned}\quad \alpha,\beta\in[0,1] \tag{18c}$$

Then the integral I can be written as

$$\begin{aligned}I&=\sum_{i=1}^{Np}\int_0^1\int_0^1 O(1/r)J_S(\mathbf{s})J_P(\mathbf{s})\,dt_1\,dt_2\\ &=\sum_{i=1}^{Np}\int_0^1\int_0^1 O(1/r)J_S(\mathbf{s})J_P(\mathbf{s})J_L^{(i)}(\alpha)\,d\alpha\,d\beta\end{aligned} \tag{19}$$

where J_S has be defined in Eq. (16), J_P is the Jacobian of the transformation from $d\Gamma$ to dt_1dt_2, Np is the total number of triangles, $J_L^{(i)}=\alpha S_\Delta$ and

$$S_\Delta=|t_1^1t_2^2+t_1^2t_2^0+t_1^0t_2^1-t_1^2t_2^1-t_1^0t_2^2-t_1^1t_2^0| \tag{20}$$

which is the area of the triangle in the intrinsic coordinate space, and keeps constant over the triangle. Now, regular Gaussian integration can be used to evaluate the above integral I.

In order to deal with thin structures effectively without having to use many surface elements with very fine size, but using coarse elements with slender shape in physical space, the subdivision of a slender element is divided into several triangles and additional quadrangles, which is different from that for a regular element shown in Fig. 3. The subdivision for an irregular element is dependent on the location of the source point as well. Fig. 5 shows the subdivisions for different locations of the source point.

For each triangle, the singular integrals are calculated by the scheme discussed above, while for the quadrangles, an integration

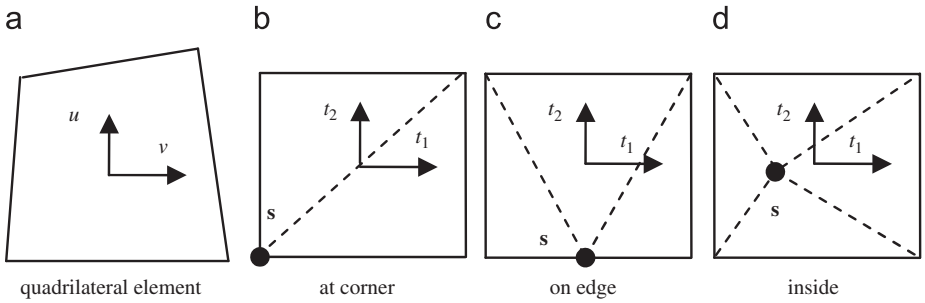

Fig. 3. A quadrilateral element and its subdivisions in the intrinsic coordinate system.

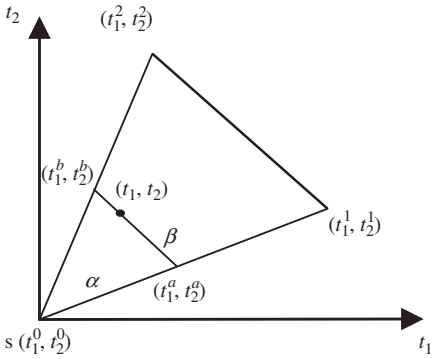

Fig. 4. Coordinate transformation.

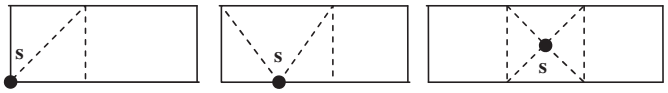

Fig. 5. Subdivisions for a slender element.

scheme for nearly singular integrals is employed, which will be discussed in next section.

4.2. Nearly singular integration

Nearly singularities arise in the BIE when slender or thin structures are considered and in cases where the boundary element distribution on a surface is very irregular, namely the densities of elements along the two coordinate directions in parametric space are very different. Accurate evaluation of nearly singular integrals is a demanding task for successful implementation of BIE analyses. So far many techniques for dealing with nearly singular integrals have been proposed [14–23]. Some of them are effective but involve complicated mathematic transformations of the integrals for a specific fundamental solution. To provide a general approach that is independent of the problem to be solved, here we developed an adaptive integration scheme based on the element subdivision method.

In this scheme, we first calculate the maximal boundary length of the integration element, l, and the distance between the source point and the center of the surface element, d, in the physical space Ω. If l is smaller than kd (k is experiential factor, $k=4$ used in the scheme) this element is taken as a regular integration patch, or it is divided into two or three or four equal sub-patches considering its shape in physical space (see Fig. 6). Then for each sub-patch, we repeat the above procedure until all patches become regular. Finally, using Gaussian quadrature for all patches, we can evaluate the integrals in Eq. (11) very accurately even when the source point is very close to the integration elements. The subdivided patches of a same element change for different source points. It should be pointed out that the surface elements are not like the elements defined in physical space used in BEM and FEM. Subdivision process is implemented easily in parametric surface space. Moreover, geometric information for a sub-patch is also derived from the face where the element is located, thus the exact geometry is kept.

5. MESH generation based on the advancing front method

For the BFM, the mesh is constructed by surface elements in the parametric space $\tilde{\Omega}$ for each surface. Therefore, the mesh used

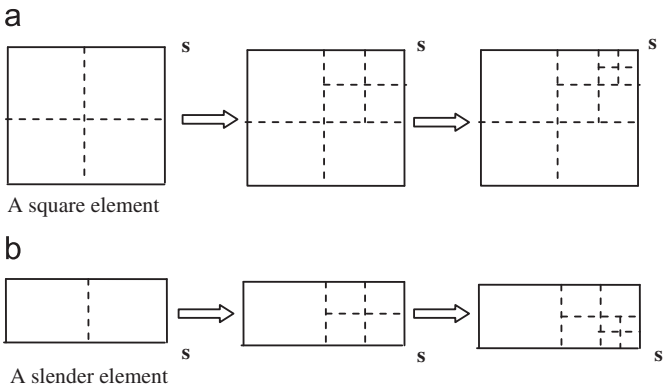

Fig. 6. Subdivisions for different elements corresponding to a source point.

for the BFM analysis is unavailable from so far existing mesh generation softwares, such as HyperMesh. In this work, an improved mesh generation method is presented for creating adaptive triangular or quadrangular surface elements over parametric surface based on the advancing front method (AFM) [9,10]. Surface elements are generated along with a quad-tree procedure to control the element size. Special care has been taken to generate elements with possibly the best shape in the space Ω during the advancing front. A local mesh improvement procedure is employed to enhance the quality of the mesh so that the obtained elements finally are suitable for boundary integration and variable approximation in the parametric space. The input data for present algorithm is a parametric surface and a polygonal description of the boundary of the surface to be meshed. This boundary information is given by a list of nodes defined by their parametric coordinates on the surface and a list of boundary segments (or edges) defined by their node connectivity. The overall algorithm is presented briefly next.

5.1. Quad-tree generation

A Quad-tree is created first, which is used to control element size, similar to initial background meshes. To illustrate the required steps for Quad-tree generation, a hypothetical example of a boundary input data is considered, as seen in Fig. 7(a). The brief descriptions for each step are as follows [10]:

- Quad-tree initialization based on given boundary segments (Fig. 7(b)). First define the rectangle (root cell) exactly covering all segments' end points in parametric space $\tilde{\Omega}$. Then each segment according to its length in the physical space Ω is used to determine the local subdivision depth of the quad-tree.
- Refinement to force a maximum cell (Fig. 7(c)). The quad-tree is refined to guarantee that no cell in its interior is larger the largest cell at the boundary.
- Refinement to balance the Quad-tree (Fig. 7(d)). This additional refinement forces only one or zero level of tree depth between neighboring cells and provides a natural transition between regions of different degrees of mesh refinement.

It is noted that the quad-tree is constructed by cells, and each cell that is defined in parametric surface is well-shaped in physical space. Local mesh generation is guided by cells according to their size.

5.2. Advancing front method

The AFM has been successfully applied to the finite element method generating surface meshes in many CAE software packages. In our work, the method combined with a Quad-tree procedure is used to subdivide parametric surface into surface elements for the BFM pre-processing. As with any advancing front method, the algorithm begins with a set of boundary segments, defined as the initial "front", Elements (triangles or quadrilaterals) are constructed one by one from the front segments and grow towards the interior of the surface. The details for implementation of the algorithm are given in Ref. [9]. However, surface elements along the surface boundary are not well-shaped generated by their methods usually, because an element is created only based on a shortest segment that is made up of new element boundaries, without taking special care along surface boundary (Fig. 8(a)). To improve these elements, a new procedure of advancing fronts is carried out here. Namely, surface elements are created by layer and layer on the boundary (Fig. 8(b)), and a shortest segment is picked as a current front among advancing fronts. The inner elements are also constructed easily like conventional methods.

Finally, the local mesh smoothing technique derived from Ref. [10] is used to improve mesh quality by relocating nodes within an element.

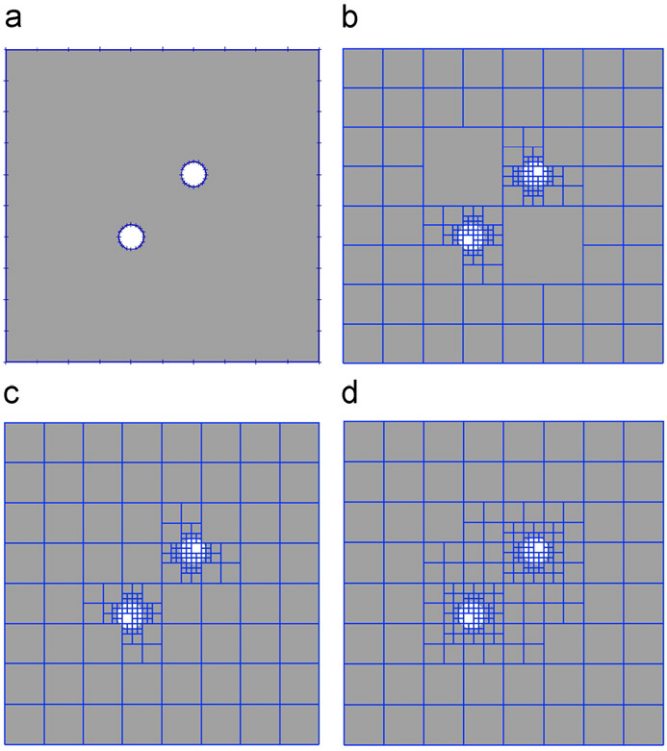

Fig. 7. Generation of quad-tree structure from a given boundary refinement.

6. Illustrative numerical results

The method has been tested for three types of 3-D geometrical objects: a torus, a slim solid and an actual machine part. The first object is used to compare our method with conventional BEM on accuracy and convergence performance. The slender bar with four small holes is presented here as a second example, to demonstrate that our method is able to use unstructured mesh, and has a capacity to deal with the problem involving fine features or thin structures. And the last one, a more geometrically complicated one, is added to verify the applicability of our method to engineering problems. The latter two objects are original CAD models, which are directly used for BFM analyses. It may be seen that our method has real potential to seamlessly interact with CAD software, and provide a new way toward automatic simulation with complicated solids. In order to assess the accuracy of the method, we have used the following cubic analytical field:

$$u = x^3 + y^3 + z^3 - 3yx^2 - 3xz^2 - 3zy^2 \tag{21}$$

In all cases, Laplace's equation is solved, together with appropriately prescribed boundary conditions corresponding to the above analytical solution.

For the purpose of error estimation and convergence study, a 'global' L_2 norm error, normalized by $|v|_{\max}$ is defined as follows [1]:

$$e = \frac{1}{|v|_{\max}} \sqrt{\frac{1}{N} \sum_{i=1}^{N} (v_i^{(e)} - v_i^{(n)})^2} \tag{22}$$

where $|v|_{\max}$ is the maximum value of u or q over N sample points, the superscripts (e) and (n) refer to the exact and numerical solutions, respectively.

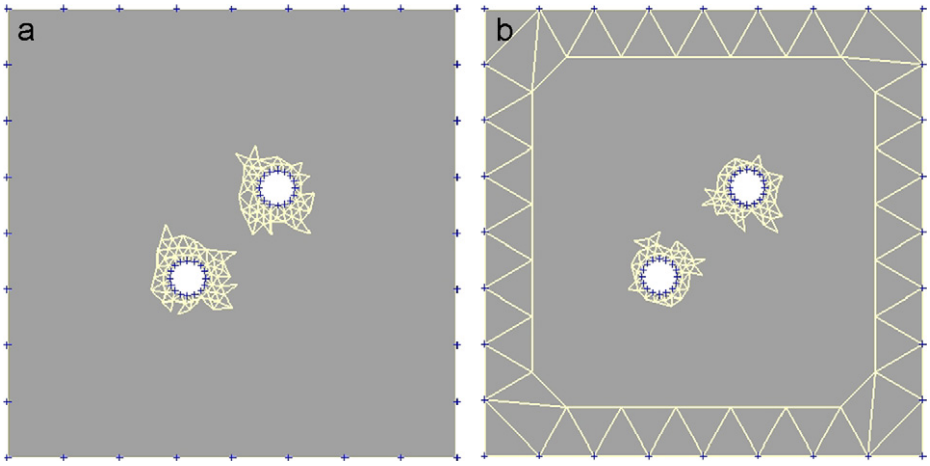

Fig. 8. Different ways to control elements generation.

Table 1
Comparison of relative errors and the computational time results between BFM and BEM.

Total elements	104	150	256	352	520	770	1330	2136	2910
Total nodes	71	98	157	210	302	436	733	1153	1557
BFM									
FErr_q(%)	4.773	4.215	3.233	2.699	2.083	1.553	1.030	0.737	0.583
FMat_t(s)	<1	<1	<1	<1	<1	1	1	2	4
BEM									
EErr_q(%)	23.48	13.55	8.181	5.459	4.006	2.811	1.803	1.231	0.927
EMat_t(s)	<1	<1	<1	<1	<1	<1	<1	2	4

6.1. Dirichlet problem on a torus

The first example considers a problem in a torus centered at origin, whose exterior radius and interior radius are 10 and 3 units, respectively. The usual ring polar coordinates θ and ϕ are used. The example is presented here to verify the accuracy and convergence performance of the BFM in comparison with the conventional BEM. The Dirichlet boundary condition corresponding to the exact solution (Eq. (21)) is imposed on the surface of the torus. Field variables are approximated by linear triangular elements. The results have been obtained for nine sets of elements listed in Table 1. Fig. 9 shows the torus discretization for the BFM analyses with 520 surface elements and 302 nodes.

The L_2 errors of nodal values of q evaluated using Eq. (22), and time required for constructing the coefficient matrices are presented in Table 1. In the table, symbols FErr_q and EErr_q denote the results from BFM and BEM, and FMat_t and EMat_t denote CPU seconds used by BFM and BEM, respectively. It is noted that the CPU time for constructing the matrices by the two methods is almost the same with respect to different set of elements.

For greater clarity, Fig. 10 shows how the L_2 errors are affected by the different method with the same number of elements. It clearly shows that our method can obtain more accurate results than conventional BEM with the same number of elements, and the convergence rate is faster than the BEM, namely numerical solutions are more stable. It is also concluded from Fig. 10 that our method is less sensitive to the mesh density than the BEM and can obtain acceptable results with a few elements. For example, the result relative error is only 4.773% obtained by the BFM with 104 triangular elements, while the relative error shoots up to 23.48% obtained by the BEM with the same number of elements. These results are reasonable, because in the BFM the geometric data at Gaussian quadrature points are calculated directly from the faces rather than from elements through interpolation, thus no geometric error will be introduced no matter how coarse the mesh is.

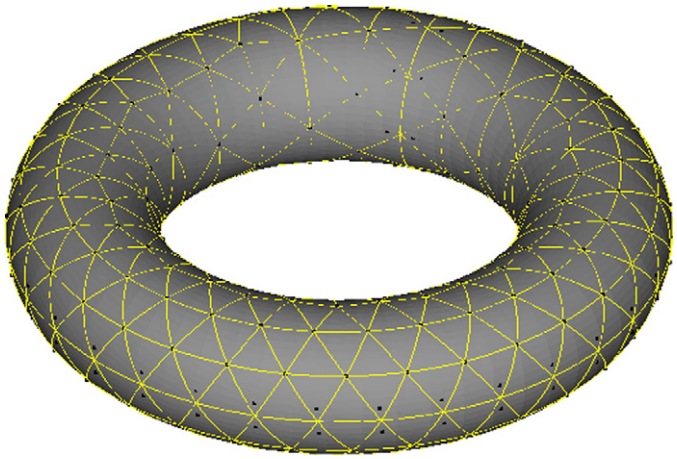

Fig. 9. The torus discretization for the BFM.

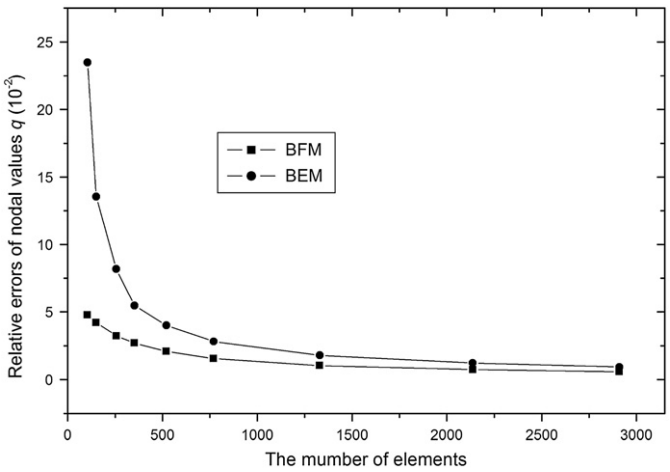

Fig. 10. Relative error against number of elements by BFM and BEM.

6.2. Mixed problem on a slender bar with four small holes

The case of the field for a slender bar with four very slim cylinder holes governed by Laplace's equation is presented as the second example. The solid and its main sizes are shown in Fig. 11. Four long and small holes are parallel to z-axis of coordinate system, and very close to each other. A boundary value problem with mix boundary conditions has been solved for the solid. The cubic exact solution has been used here (Eq. (21)). The natural boundary conditions are imposed on the two end faces $z=\pm 50$ of the bar, and the essential boundary conditions on all other faces.

Variables are approximated by linear triangular elements on two end surfaces trimmed by small holes, and variables on any other surfaces are approximated by quadratic quadrilateral elements. Those elements are created by an adaptive mesh generation scheme described in Section 5 (see Fig. 12). Well-shaped elements with smooth fine to coarse transition are obtained for trimmed surfaces (see Fig. 13). The numerical results have been obtained using 948 elements and 1236 nodes. The L_2 errors of nodal values for u and q are 0.023% and 0.280%, respectively. Figs. 15 and 16 show results of the potential and its directional derivative at the inner points (see Fig. 14) located on the line segment from $(0, 0, -48)$ to $(0, 0, 48)$ inside the bar, respectively. The gradient is dotted with the z-axis in order to get the directional derivative along this line. Values of u and q, at internal points close to the surface of the body, are calculated by the nearly singular integration scheme described in Section 4.2. It is seen that results are accurate even when the points are very close to the boundary.

Numerical results of the normal flux q of the boundary points (see Fig. 14) are shown in Fig. 17. Those points are located along the line segment from $(0.1616, -0.1892, -49)$ to $(0.1616, -0.1892, 49)$ on a slim cylindrical surface. It is seen that the

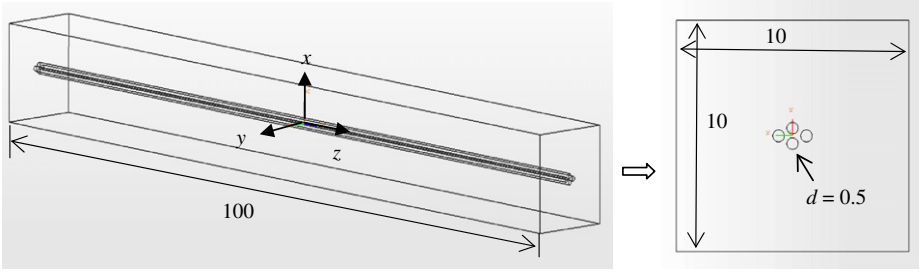

Fig. 11. The slender bar and its main sizes.

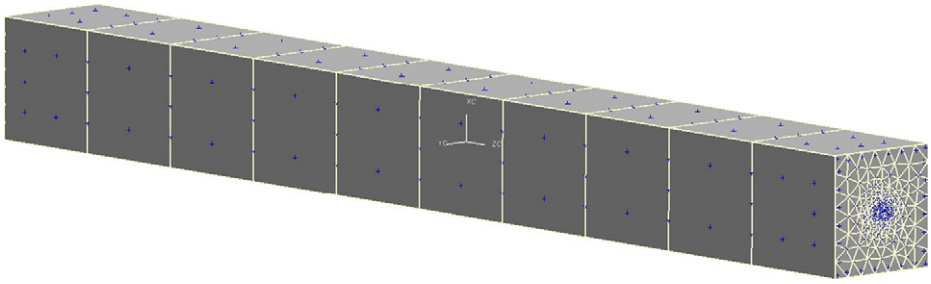

Fig. 12. The BFM discretization for the slender bar.

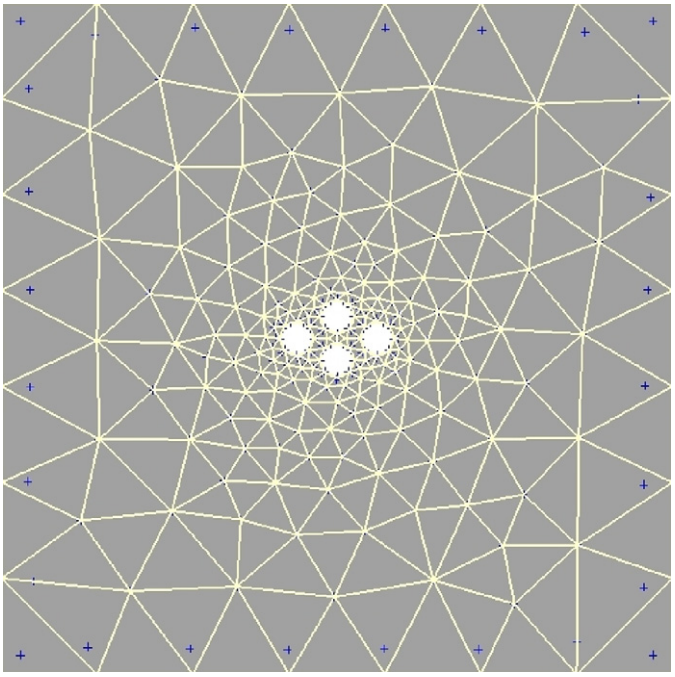

Fig. 13. Mesh for the surface trimmed by small holes.

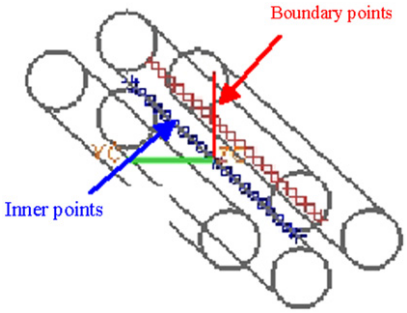

Fig. 14. Evaluation points. Boundary points located at one of cylindrical surfaces, while inner points inside the bar close to four cylindrical surfaces equally.

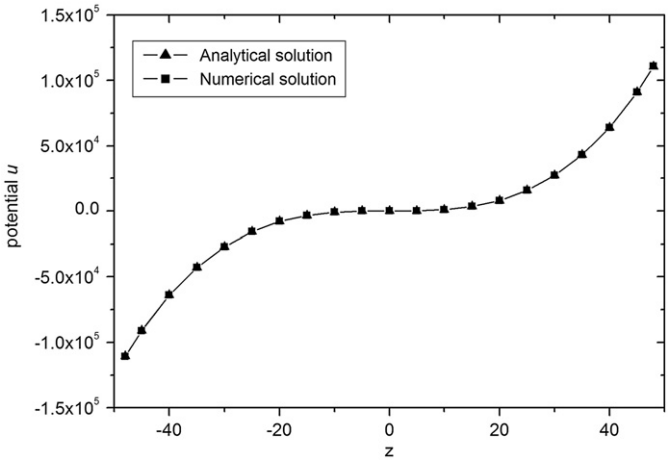

Fig. 15. Results of potential u for inner points.

numerical results are in good agreement with the analytical solution.

It may be noted here that approximation variables between two surfaces bounds are discontinuous, yet values in the interior of each surface are continuous, and the nodal values to be smoothed in the post-procedures afterward. This provides a more flexible way to constructed meshes for each surface independently. So fine meshes are only used near detailed configurations on a trimmed surface, and ordinary meshes are created according to global mesh controlled size. A few slim meshes on a slim surface are generated without having to use many smaller elements. Moreover, in our method, we do not use elements to approximate the geometry. The coarse mesh constructed by surface elements can keep exact geometric information. Thus, it is efficient to deal with any slim or thin structures meshed by slim surface elements for the simulation 3-D potential problems. In this example, four slim cylindrical surfaces are discretized by very slim quadrilateral elements. For each element, adaptive

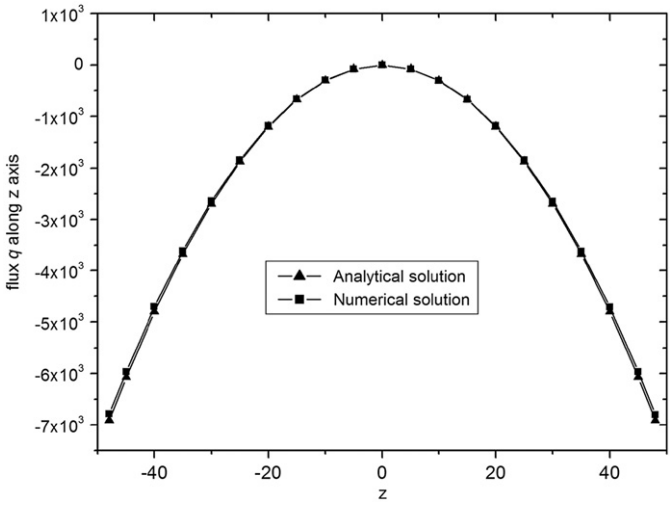

Fig. 16. Results of directional derivative of potential u for inner points.

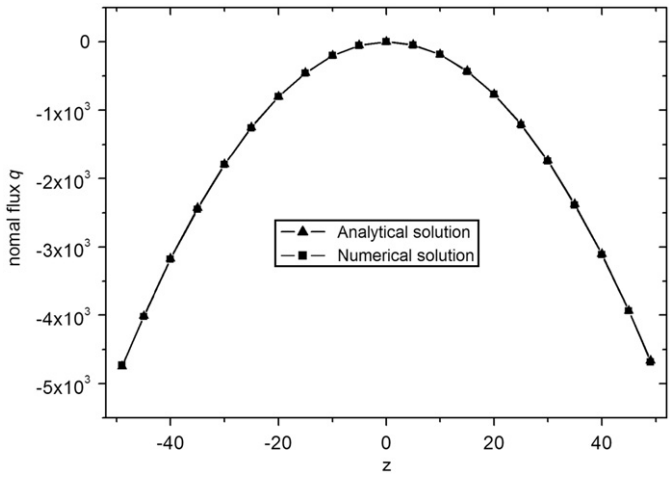

Fig. 17. Normal flux q at boundary points.

integration schemes based on the element subdivision method are carried out, discussed in Section 4. The obtained numerical results have indicated the adaptive integration schemes are effective.

6.3. Dirichlet problem on a real mechanical part

The problem of a real mechanical part with complicated geometry is solved here. The part is modeled with boundary representation (B-rep) data structure obtained from the commercial CAD software UG-NX(R), shown in Fig. 18. As the BFM is implemented based on the B-rep structure directly, we can develop an interface between BFM and UG-NX(R) easily. All geometric information as well as topology relations used for mesh generation and BFM analysis is available by accessing to program functionality from the UG Open Architecture. Using the combined software, an analysis on a real mechanical part is automatically conducted.

The boundary of the mechanical part is discretized directly on the CAD model by 2281 surface elements and 2439 nodes (see Fig. 19). The essential boundary conditions are imposed on all faces corresponding to the analytical solution (Eq. (21)). Variables

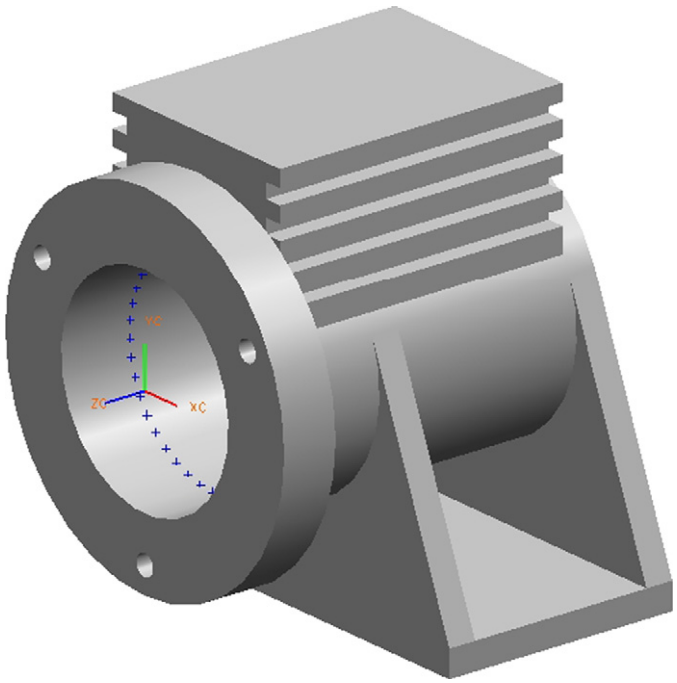

Fig. 18. A mechanical part with complicated geometry.

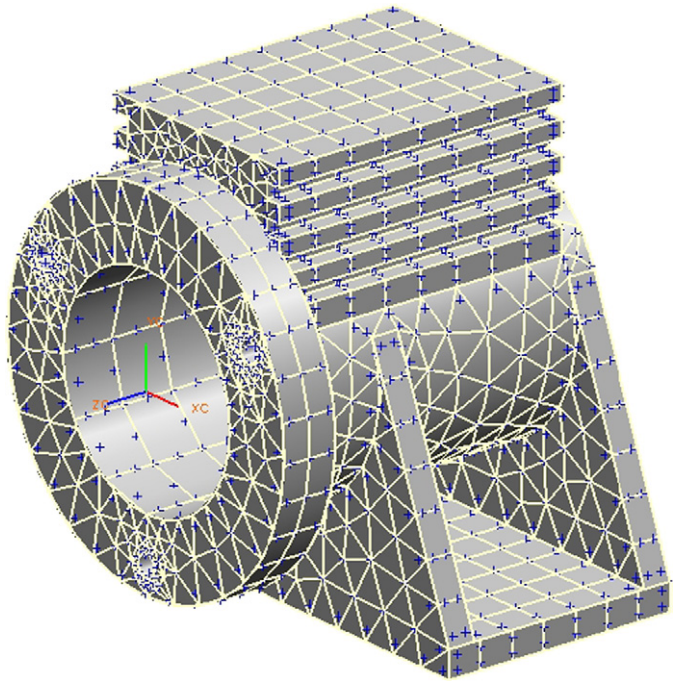

Fig. 19. BFM discretization for the mechanical part.

are approximated by quadratic elements for the cylindrical surface on which the evaluation points are located (see Fig. 19), and for any other surfaces by linear triangular elements.

The numerical L_2 errors of nodal values q is 1.54%, indicating the integration of the BFM and UG-NX(R) is successful, and our method is capable of dealing with the problems with complicated geometry. Numerical results of normal flux q of the points located on the cylindrical surface are shown in Fig. 20. It is seen that numerical results are in agreement with analytical solution.

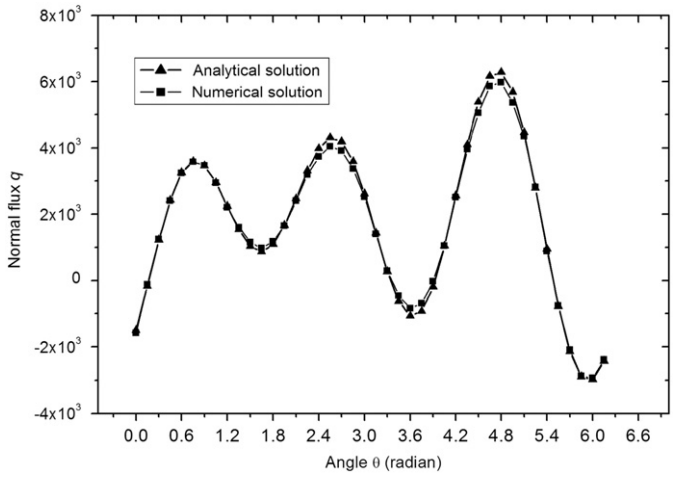

Fig. 20. Normal flux q of the points located on a cylindrical surface.

7. Conclusions

The BFM has been implemented with surface elements on the geometry directly for solving 3D potential problems. The method provides a new implementation of the BEM. In this method, no conventional elements are used for boundary integration or geometric approximation. The boundary integration is performed using surface elements, which are constructed in the parametric space of each boundary face. The integral quantities, such as the coordinates of Gaussian points, the Jacobian, and the out normal are calculated from the bounding surface using the geometric map between the physical space and the parametric space, thus no geometric errors are introduced. The variable approximation scheme in parametric space based on elements has been developed, allowing for a consistent way to allow both continuous and discontinuous surface elements to coexist in the same BFM model. Adaptive integration scheme for nearly singular integrals and adaptive mesh generation method based on the AFM combined with a quad-tree, have also been developed.

The BFM has been verified through a number of numerical examples with different geometries, boundary conditions types corresponding to a cubic analytical solution. It was observed that our method can get more accurate numerical results than the conventional BEM, and is less sensitive to the mesh density. The solution is accurate for the potentials and fluxes on the boundary and inside the domain even with features in small size.

Numerical examples involving complicated geometry have demonstrated that the integration of the BFM and commercial software UG-NX(R) is successful. The BFM provides a natural way to integrate geometric design and engineering analysis into a completely unified framework. Developing an analysis tool with the BFM based on CAD modeling packages and combining the BFM with the fast multipole method [24,25] to solve large scale practical problems are undergoing.

Acknowledgements

This work was supported in part by National Science Foundation of China under grant number 10972074, in part by National 863 Program of China under grant number 2008AA042507, and in part by National 973 Project of China under grant number 2010CB328005. The authors would like to thank Dr. Liu Yijun for helpful comments and suggestions which have improved the quality of the paper.

References

[1] Zhang JM, Qin XY, Han X, Li GY. A boundary face method for potential problems in three dimensions. Int J Numer Meth Eng 2009;80:320–37.
[2] Mukherjee YX, Mukherjee S. The boundary node method for potential problems. Int J Numer Meth Eng 1997;40:797–815.
[3] Zhang JM, Yao ZH, Li H. A hybrid boundary node method. Int J Numer Meth Eng 2002;53:751–63.
[4] Liu GR, Gu YT. An introduction to mesh free methods and their programming. Dordrecht, The Netherlands, USA: Springer; 2005.
[5] Liu CS. An effectively modified direct Trefftz method for 2D potential problems considering the domain's characteristic length. Eng Anal Bound Elem 2007;31:983–93.
[6] Kagan P, Fischer A. Integrated mechanically based CAE system using B-Spline finite elements. Comput-Aid Design 2000;32:539–52.
[7] Hughes TJR, Cottrell JA, Bazilevs Y. Isogeometric analysis: CAD, finite elements, NURBS, exact geometry and mesh refinement. Comput Methods Appl Mech Eng 2005;194:4135–95.
[8] Wang L. Integration of CAD and boundary element analysis through subdivision methods. Comput Ind Eng 2009;57(3):691–8.
[9] Lee CK, Hobbs RE. Automatic adaptive finite element mesh generation over rational B-spline surfaces. Comput Struct 1998;69:577–608.
[10] Miranda AC, Meggiolaro MA. Castro JTP. Fatigue life and crack path predictions in generic 2D structural components. Eng Fract Mech 2003;70:1259–79.
[11] Shaw Amit, Roy D. NURBS-based parametric mesh-free methods. Comput Methods Appl Mech Eng 2008;197:1541–67.
[12] Kane JH. Boundary element analysis in engineering continuum mechanics. Englewood Cliffs: Prentice-Hall Inc; 1994.
[13] Bazilevs Y, Calo VM, Cottrell JA, Evans JA, Hughes TJR, et al. Isogeometric analysis using T-splines. Comput Methods Appl Mech Eng 2010;199:229–63.
[14] Chati MK, Mukherjee S. The boundary node method for three-dimensional problems in potential theory. Int J Numer Meth Eng 2000;47:1523–47.
[15] Nagaranjan A, Mukherjee S. A mapping method for numerical evaluation of two-dimensional integrals with $1/r$ singularity. Comput Mech 1993;12:19–26.
[16] Liu YJ. Analysis of shell-like structures by the boundary element method based on 3-D elasticity: formulation and verification. Int J Numer Meth Eng 1998;41:541–58.
[17] Luo JF, Liu YJ, Berger EJ. Analysis of two-dimensional thin structures (from micro- to nano-scales) using the boundary element method. Comput Mech 1998;22:404–12.
[18] Chen XL, Liu YJ. An advanced 3-D boundary element method for characterizations of composite materials. Eng Anal Bound Elem 2005;29(6):513–23.
[19] Liu YJ, Zhang DM, Rizzo FJ. Nearly singular and hypersingular integrals in the boundary element method. In: Brebbia CA, Rencis JJ, editors. Boundary elements XV. Worcester, MA: Computational Mechanics Publications; 1993. p. 453–68.
[20] Niu ZR, Cheng CZ, Zhou HL, Hu ZJ. Analytic formulations for calculating nearly singular integrals in two-dimensional BEM. Eng Anal Bound Elem 2007;31:949–64.
[21] Chen HB, Lu P, Huang MG, Williams FW. An effective method for finding values on and near boundaries in the elastic BEM. Comput Struct 1998;69(4):421–31.
[22] Chen JT, Hong HK. Review of dual boundary element methods with emphasis on hypersingular integrals and divergent series. Appl Mech Rev 1999;52(1):17–33.
[23] Gao XW, Yang K, Wang J. An adaptive element subdivision technique for evaluation of various 2D singular boundary integrals. Eng Anal Bound Elem 2008;32:692–6.
[24] Zhang JM, Masa Tanaka, Endo M. The hybrid boundary node method accelerated by fast multipole method for 3D potential problems. Int J Numer Meth Eng 2005;63:660–80.
[25] Zhang JM, Masa Tanaka. Adaptive spatial decomposition in fast multipole method. J Comput Phys 2007;226:17–28.